Version 8

Running title: New structure of high-pressure body-centered orthorhombic Fe_2SiO_4

Takamitsu Yamanaka[1], Atsushi Kyono[1,3], Yuki Nakamoto[1,4], Svetlana Kharlamova[1], Viktor V. Struzhkin[1], Stephen A. Gramsch[1], Ho-kwang Mao[1,2] and Russell J. Hemley[1]

Washington, D.C. 20015 USA

[2] *High Pressure Collaborative Access Team, Geophysical Laboratory, Carnegie Institution of Washington, Argonne, Illinois, 60439, USA*

[3] *Division of Earth Evolution Sciences, Graduate School of Life and Environment Sciences, University of Tsukuba, Tsukuba Ibaraki 305-8572 Japan*

[4] *Center for Quantum Science and Technology Under Extreme Conditions, Osaka University, Toyonaka Osaka, 560-8531 Japan*

Corresponding Author: Takamitsu Yamanaka
tyamanaka@ciw.edu

Abstract

A structural change in Fe_2SiO_4 spinel (ringwoodite) has been found by synchrotron powder diffraction study and the structure of a new high-pressure phase was determined by Mote-Carlo simulation method and Rietveld profile fitting of x-ray diffraction data up to 64 GPa at ambient temperature. A transition from the cubic spinel structure to a body centered orthorhombic phase (*I*-Fe_2SiO_4) with space group *Imma* and Z=4 was observed at approximately 34 GPa. The structure of *I*-Fe_2SiO_4 has two crystallographically independent FeO_6 octahedra. Iron resides in two different sites of six-fold coordination: Fe1 and are arranged in layers parallel to (101) and (011) and are very similar to the layers of FeO_6 octahedra in the spinel structure. Silicon is located in the six-fold coordination in *I*-Fe_2SiO_4. The transformation to the new high-pressure phase is

reversible under decompression at ambient temperature. A martensitic transformation of each slab of the spinel structure with translation vector $<\vec{1/8}\ \vec{1/8}\ \vec{1/8}>$ generates the *I*-Fe_2SiO_4 structure. Laser heating of *I*-Fe_2SiO_4 at 1500 K results in a decomposition of the material to rhombohedral FeO and SiO_2 stishovite. Fe $K\beta$ x-ray emission measurements at high pressure up to 65GPa show that the transition from a high spin (HS) to an intermediate spin (IS) state begins at 17 GPa in the spinel phase. The IS electron spin state is gradually enhanced with pressure. The Fe^{2+} ion at the octahedral site changes the ion radius under compression at the low spin, which results in the changes of the lattice parameter and the deformation of the octahedra of the spinel structure. The compression curve of the lattice parameter of the spinel is discontinuous at approximately 20 GPa. The spin transition induces an isostructural change.

Keywords

New high-pressure structure, Fe_2SiO_4 ringwoodite, x-ray emission spectra, spin transition, martensitic transition.

Introduction

A great deal of attention has been paid to the high-pressure structural transitions of the many spinel phases present in the Earth's crust due to their geophysical importance (Akimoto and Fujisawa, 1967; Basset and Ming, 1972; Ito and Takahashi, 1987; Irifune et al. 1998). One of the major minerals in the crust, $(Mg,Fe)_2SiO_4$ olivine (α-phase), transforms to wadsleyite (β-phase, modified spinel) and further to ringwoodite (γ-phase, spinel). These transitions were proposed for the origin of the seismic discontinuity of the transition zone from 410 km to 660 km depth (Ringwood and Irifune, 1988). These high-pressure transformations have been studied from various viewpoints, including the electronic and elastic properties of participating phases (Kiefer et al. 1997; Li et al. 2007) and continue to provide significant information for seismic interpretation (Leven et al. 1981; Burnley et al. 1991; Shim et al. 2001).

Recently Fe_2SiO_4 phase with spinel structure was found in meteorite and Silicate spinels of transition elements are investigated for their influence on the magnetic and electrical properties of the Earth's crust and mantle. Their phase stabilities and structures under high-pressure and high-temperature conditions have been

intensively studied. Phase relations in the Mg_2SiO_4-Fe_2SiO_4 ringwoodite solid solution system have been investigated in numerous high-pressure studies (Katsura et al., 1989; Ito and Takahashi. 1989; Fei et al., 1999; Matsuzaka et al, 2000). Mechanisms for the polymorphic transformations of the α, β and γ phases of (Mg, have been discussed in terms of the observation of dislocations by TEM (Price et al. 1982; Madon and Poirier 1983). Structures of silicate spinels M_2SiO_4 (M= Mg, Fe, Co, Ni) have been refined from x-ray diffraction data at ambient conditions (Yagi et al. 1974; Morimoto et al. 1970, 1974; Ma, 1975; Marumo et al. 1974, 1977). (1981). End member of ringwoodite solid solution, Fe_2SiO_4, undergoes transitions at 6.4 GPa at 1700℃ (Yagi et al., 1987). Further experimental studies have been undertaken by Fei et al., (1991) and Matsuzaka a (2000).

Significant work is also focused on the physical properties of iron-bearing spinels in order to understand their strong electronic correlations as manifested in charge transfer, electron hopping and the Jahn-Teller effect, in particular through magnetic and electrical conductivity measurements and Raman spectroscopy l. 1998; Woodland and Angel, 2000; Woodland et al., 2010; Yamanaka et al., 2001a, 2001b; et al., 2004).

Recently, at pressures above 30 GPa and ambient temperature, a pseudo-rhombohedral phase of Fe_2SiO_4 was proposed as high-pressure phase by powder diffraction and Mössbauer spectroscopy measurements (Greenberg et al., 2011). It has been reported that the spinel phase of Fe_2SiO_4 decomposes to FeO (wüstite) and SiO_2 (stishovite) at higher pressures (Katsura and Ito, 1989; Ito and Takahashi, 1989), because the Si atom is too small make any of the post-spinel phases stable at high pressure (Ito and Takahashi. 1989).

Single crystal structure analyses of Fe_2SiO_4 spinel have been carried out using a diamond anvil cell up to 8.9 GPa by Hazen (1993) and up to 10.2 GPa (2011). Lattice dynamics and thermodynamic properties of antiferromagnetic Fe_2SiO_4 spinel were determined using phonon dispersion curves from density functional theory at pressures up to 20 GPa (et a et al., 2011).

Electronic spin transitions attributed to change from the high-spin (HS) to low-spin (LS) states in transition metals, particularly iron, have been increasingly used to understand anomalies in the properties of oxides and silicates at high pressure. X-ray emission spectroscopy (XES), carried out using a synchrotron source and DAC techniques, is a method for probing the spin state of iron at high pressures et al., 2007; Li et al., 2004, Lin et al., 2005). The spin state change of Fe^{2+} in the octahedral site is accelerated at higher pressures.

In the present experiment, the details of the structural transformation of Fe_2SiO_4 ringwoodite due to an electronic spin transition were elucidated by x-ray diffraction and x-ray emission measurements up to 64 GPa at

ambient temperature. A new high-pressure phase was determined to have a body-centered orthorhombic structure in space group *Imma* (z = 4) rather than rhombohedral $R\bar{3}m$, which was previously proposed by Greenberg et al., (2011). The correlation between the structural transition and the spin state is also investigated by XES experiment. .

Experimental Methods

Synchrotron x-ray Diffraction and structure analysis

Fe_2SiO_4 spinel was prepared using a multianvil high-pressure apparatus。 A mixture of Fe_2O_3 and SiO_2 was heated at 1500 °C for five hours under an atmosphere of CO_2 and H_2 with a mixing ratio of 1/1. The quenched sample was confirmed to be fayalite Fe_2SiO_4, which then served as the starting material for a high-pressure synthesis of the spinel phase. The powdered fayalite was placed directly into a cylindrical graphite heater that was set at the center of an octahedral pressure medium. The synthesis conditions were 8 GPa and 1400 ℃ for 1 hour, employing the Kawai-type multianvil apparatus installed at ISEI, Okayama University. The graphite heater prevented oxidation to ferric iron. The product was confirmed to be single-phase spinel by electron micro probe analyzer and powder x-ray diffraction.

Angle-dispersive powder x-ray diffraction was carried out using synchrotron radiation with wavelength 0.4262 Å at beam line 16-BM-D at the Advanced Photon Source (APS), Argonne National Laboratory. A highly focused x-ray beam with 2 mm in diameter was aligned with the center of the sample chamber in the diamond-anvil cell (DAC). The diffraction patterns of the samples were recorded with an imaging plate (MAR-345) and processed with FIT2D software (http://www.esrf.fr/computing/scientific/FIT2D/). The detector tilting and the distance between the sample and detector were calibrated against the known lattice parameters of CeO_2. The lattice parameters of the samples were determined by fitting the observed diffraction peaks. A symmetric diamond anvil cell (DAC) was prepared with diamonds having culet and 450 in diameter. The sample chamber consisted of a hole drilled in a rhenium gasket with initial thickness of 200 μm and to 60 μm. The fine powder spinel sample, together with a ruby chip for a pressure marker, was loaded in the sample chamber. Ne served as the pressure medium and was loaded into the cell using a gas loading apparatus. Pressure was determined by the ruby luminescence method (et al., 1975; Mao et al., 1986). An off-line laser heating system in the double-sided configuration, and consisting of a laser along with associated optics, was used to heat

the sample. The temperature during laser heating was approximately 1500 K, which was determined using spectral radiometry based on the Planck radiation function.

For the diffraction patterns of two-phase mixture over 39 GPa, the lattice parameters were obtained using the DICVOL, indexing routine (Boultif and Louer, 2004), with about 12 reasonable and strong reflections in range 2□= 4° - 20°. Subsequently, a Monte-Carlo method was applied to find candidates for the high-pressure structure using the diffraction intensities with fixed lattice parameters as determined by DICVOL. Rietveld profile fitting was then performed with the program RIETAN-2000 (Izumi and Ikeda, 2000) using the initial model observed from the Mote-Carlo simulation. To fit the data, the background intensity distribution was first adjusted for the refinement. Lattice parameters, atomic positional coordinates and temperature factors were treated as variable parameters. Subsequently, profile parameters (full width at half maximum, asymmetry parameters and angular decay parameter) were varied in the refinement. A preferred orientation correction was made considering the spinel cleavage habit. Finally a full matrix, least-squares refinement was conducted.

X-ray Emission Spectroscopy (XES)

X-ray emission spectra (XES) measurements on Fe_2SiO_4 were carried out up to 65 GPa at ambient temperature at beam line 16-ID-D APS. The spin state of ferrous iron is characterized by the appearance of a satellite emission peak located in the lower energy region of the main emission peak which is a result of the 3*p*–3*d* core–hole exchange. The experimental setup and specifications of the apparatus are described in a previous report (Yamanaka et al., 2013). A panoramic DAC, with a configuration similar to that used in the synchrotron diffraction experiments was prepared for the XES measurements, except that a Be gasket was used instead of an Re gasket.

We applied the variation of the spin state through the integrated absolute values of the difference spectra (IAD et al., 2006). The high-spin (HS) and low-spin (LS) spectral functions are normalized to unit area at integration. The IAD value for the complete spin transition can be given as $IAD_{HL} = \int |h(E) - l(E)|$ A spectrum in the transition region is a superposition of those of the two spin states, thus it can be expressed as $s = \gamma + (1 - \gamma_{HS})$ is the high-spin fraction. Its difference from the low-spin reference l is $s - l = \gamma_{HS}(h - l)$. The integral of its absolute value is

$$\mathrm{IAD}(s) = \int |s(E) - l(E)| dE = \gamma_{\mathrm{HS}} \mathrm{IAD}_{\mathrm{HL}}$$

141 The IAD is proportional to a fraction of the high spin and is a good indicator of the amount of the transition.

142

143 ## Results

144 Compression of the lattice parameter Fe_2SiO_4 spinel and structure transition

145 Selected powder diffraction patterns obtained at increasing pressures up to 54.6 GPa at ambient
146 temperature are shown in Fig. 1. Up to 34.8 GPa, the patterns show a single phase with the spinel structure. A
147 new pattern, different from that of the spinel phase, was observed above 38.8 GPa, although the spinel pattern
148 was detected even at 54.6 GPa as a residual phase.

149 In Fe_2SiO_4 spinel, Si is located in the tetrahedral site and Fe on octahedral sites, resulting in a normal
150 spinel with space group $\bar{3}m$. Only two parameters, the oxygen positional parameter u and the lattice
151 parameter a, are variables in the structure refinement. The lattice parameter and density as determined from
152 the Rietveld refinement are presented in Table 1 in which those data of the residual spinels over 38.8 GPa are
153 also presented. The variation in the lattice parameters of spinel phase with pressure is illustrated in Fig. 2. The
154 parameter shows two distinct regimes of compression behavior, one in a lower pressure region between
155 ambient pressure and 20 GPa, and another above the pressure. The Si-O and Fe-O distances are presented
156 in Table 2. The Si-O and Fe-O distances and the volume of tetrahedron (SiO_4) and octahedron (FeO_6) are
157 calculated from the Rietveld analysis. The variations of the volume ratios of these sites SiO_4) and R(FeO_6)
158 with pressure are shown in Fig. 3. The bulk modulus was calculated using the third-order (BM) equation of
159 state (Birch, 1947). In the lower pressure region between ambient pressure and 20 GPa, the bulk modulus is
160 K_0 = 177 (10) GPa and K_0' = 8.8 (1.9), while in the high-pressure region between 20 GPa and 54.6 GPa, K_0 =
161 209 (8) GPa and K_0' = 3.8 (0.5). Overall data all through pressures are K_0 = 200(9) GPa and K_0' = 4.3(7).
162 These data are similar to the previous data: K_0 = 201(8) GPa, K_0' = 3.7(7) (Greenberg et al, 2011) and K_0 =
163 204.5(7) GPa, K_0' = 4.3(3) (Liu et al., 2008), and K_0 = 202(4) GPa, K_0' = 4

164 Diffraction patterns obtained under decompression from 54.6 GPa down to 31.0 GPa are shown in Fig. 4,
165 and reveal the back-transformation from the high-pressure phase to the spinel phase, indicating a reversible
166 transition. After the back-transformation, the spinel phase was heated to 1500 K, resulting in a decrease in
167 pressure from 33 GPa to 31 GPa. The diffraction pattern taken at 31 GPa shows partial decomposition of the
168 spinel to rhombohedral FeO and SiO_2 stishovite together with residual spinel. It is probable that a longer heating

169 period would enhance this decomposition. The recovered sample was again compressed to 55 GPa at ambient
170 temperature, and the residual spinel transformed again to the high-pressure phase. The decomposition process
171 confirmed the disproportionation of Fe_2SiO_4 to $2FeO + SiO_2$, reported by Bassett and Ming (1972).
172
173 Orthorhombic high-pressure phase of Fe_2SiO_4
174 Rietveld profile fitting analysis of the diffraction patterns taken at 44.6 GPa and 54.6 GPa at ambient
175 temperature indicate a two-phase mixture consisting of the new high-pressure phase and the residual spinel
176 phase. The pattern at 64 GPa confirms only high-pressure single phase without spinel phase. Greenberg et al.
177 (2011) proposed a pseudo-rhombohedral phase at pressures above 30 GPa at ambient temperature from x-ray
178 diffraction and Mössbauer data. In their structure analysis, the residual spinel phase was not considered in the
179 Rietveld refinement and provided a fit to the rhombohedral $R\bar{3}m$ structure. Several peaks in the pattern,
180 however, were not indexed or poorly fitted, as shown in Fig. 5. A fit of the data obtained at 44.6 GPa to the
181 rhombohedral structure does not result in a satisfactory refinement. On the other hand, a mixture of the
182 orthorhombic high-pressure phase and spinel fits the 54.6 GPa data quite well (Fig. 6). The diffraction pattern
183 corresponding only to the high-pressure phase was observed at 64 GPa (Fig. 7 and CIF in the supplement
184 file).
185 Rietveld analysis of the high-pressure diffraction data confirms that the new phase has a body-centered
186 orthorhombic structure with space group symmetry of *Imma* and Z=4. Hereafter the new phase is referred to
187 as *I*-Fe_2SiO_4. Iron resides in two different sites Fe1 with site symmetry of 2/create layers parallel to (101) and
188 (011) planes, and they are very similar to the octahedral layers that form (111) and $(1\bar{1}1)$ planes of the spinel
189 structure. The Fe octahedra in the spinel structure split two different F1 and Fe2 octahedra in the *I*-Fe_2SiO_4
190 structure. And the Si tetrahedra subsidiary changes the coordination to the six-fold octahedron. The
191 Mössbauer spectra of Fe_2SiO_4 taken at 61 GP by Greenberg et al. (2011) revealed two doublets indicating
192 two independent ferrous sites. The spectra are more consistent with *I*-Fe_2SiO_4 structure than their proposed
193 rhombohedral structure with only one Fe site.
194 The Si atom changes coordination from four-fold in the spinel phase to six-fold in *I*-Fe_2SiO_4 with site
195 symmetry 2/*m* (4*a*). This change in coordination results in a chain of octahedra parallel to the <100> direction
196 in *I*-Fe_2SiO_4. The octahedral arrays of SiO_6 and FeO_6 octahedra are shown in Fig. 8, and the result of the

197 structural refinement of the *I*-Fe_2SiO_4 phase is shown in Table 3. The transition is induced by atomic
198 displacements in the spinel structure, which generates the orthorhombic distortion in the *I*-Fe_2SiO_4
199 arrangement. The lattice parameters of spinel and *I*-Fe_2SiO_4 is characterized by the following the axial
200 relation:

201 This is equivalent to a martensitic transformation with translation vector of $<1/8\ \ 1/8$

202 $1/8>$ on each slab in the spinel structure, as illustrated in Fig. 9. The density of *I*-Fe_2SiO_4 at 54.6 GPa is 5.620
203 g/cm^3, about 1 % larger than that of the residual spinel phase 5.572 g/cm^3, as shown in Table 1.
204
205 Photoemission spectroscopy shows that intra-atomic interactions dominate the $K\beta$ spectral line shape.
206 $K\beta'$ and $K\beta_{1,3}$ lines shift towards each other with decreasing valence spin and (3*p*, 3d) exchange interaction
207 (Lin et al., 2005, 2007; Li et al., 2006). In previous work, we found a high-spin to intermediate-spin transition
208 in Fe_2TiO_4 at about 19 GPa (Yamanaka et al., 2013). The result and the transition pressure of Fe_3O_4 at 15.8
209 GPa (Ding et al., 2008) and) are much lower spin transition pressures as compared with magnetio-wüstite
210 and other earth materials (et al., 1999; Lin et al., 2005, 2010). X-ray emission (XES) spectra in the Fe $K\beta$
211 region for the spinel phase of Fe_2SiO_4 are presented in Fig. 10, and indicate an intermediate spin state,
212 resulting from the relative integrated intensities due to the energy shift of. The integrated absolute difference
213 (IAD) is proportional to the Fe fraction in high spin state (Venko et al., 2006). The observed electronic spin
214 transition pressure of *I*-Fe_2SiO_4 starts at about 17 GPa. This is a little lower pressure than the structural
215 transition pressure of 20 GPa observed by XRD. From the high spin (HS) to intermediate spin (IS) transition,
216 the $K\beta'$ peak intensity decreases gradually. However, an ideal low-spin state (LS) was not generated even at
217 65 GPa of the highest pressure achieved in this work. The spin transition starts at a little lower pressure than
218 the structural transition pressure of many iron-bearing oxides and silicates, as observed by x-ray diffraction.
219 For example, XES measurements on Fe_3O_4 by Ding et al. (2008) indicate that the spin transition takes place
220 at a lower pressure (15.8 GPa) than the structural change to the post-spinel phase (23 GPa). Fe_2TiO_4 also
221 undergoes a transition to an intermediate-spin state beginning at 14 GPa (Yamanaka et al., 2013).
222
223 **Discussion**
224 Pressure-induced electronic spin transitions of ferrous ion are a crucial factor in the compression behavior

of spinels, magnesiowüstite, perovskites and post-perovskites. A high-spin to intermediate-spin transition of Fe_3O_4 occurs at 15.8 GPa (Ding et al., 2008) and Fe_2TiO_4 at about 19 GPa (Yamanaka et al., 2013). Those pressures are a little lower pressure than structure transition pressure. The change in the spin state of Fe_2SiO_4 observed at approximately 17 GPa should also have a significant effect on the effective ionic radii. In the high-spin state Fe^{2+} ($3d^6$) the octahedral site at ambient conditions, two electrons reside in the doubly e_g orbital in t_{2g} orbital. In low-spin state under high-pressure conditions, one or two e_g electrons move down in energy to the t_{2g} orbital additional possibilities for *d-p-π* bonding (Fe t_{2g}–O 2*p*), but less possibilities for σ-type (Fe - O 2*p*) bonding. These ligand configuration effects combine to give a smaller effective ionic radius for the low spin state of Fe^{2+}. In the case of Fe_3O_4, the XES result can be interpreted as the spin transition at Fe^{2+} in the octahedral site, while the two Fe^{3+} remain in the high spin state.

The ionic radii reported by Shannon (1976) gives the radii for Fe^{2+} as 0.780 Å at HS and 0.61 Å at LS. The spin transition therefore reduces the ferrous ion radius by about 20 %. The Fe^{2+}-O bond distance is likewise reduced from A change in the effective ionic radius brings about a polyhedral distortion. While the Si-O bond is not easily compressed, the Fe-O bond length is reduced dramatically under compression. The observed decrease in the lattice parameter leads to the corresponding change in octahedral volume. The volume ratio of the octahedron shows a distinct change due to the compression behavior of Fe-O bond distance at 20 GPa. These discontinuous changes are induces by the spin transition, starting at 17 GPa. However, the volume of the tetrahedron does not show a noticeable change in contrast to the octahedra. Fe2 ion changes the spin state to an intermediate spin, resulting in its greater distortion of FeO_6 and smaller bond lengths, but Fe1 ion located at a larger and less distorted site probably remains in the HS state even at 64 GPa, (Table 4).

Implication of this paper

Numerous investigations of the structure transitions and decompositions of spinels have been executed under extreme conditions. Silicate spinels with transition elements or mixed-charge cations have been intensively studied from various viewpoints such as their magnetic susceptibility, electric conductivity, or elastic property.

The olivine-spinel transformation has been strongly studied for significance at the transition zone of the

253 earth's mantle. Fe_2SiO_4 has an olivine structure (α-Fe_2SiO_4, fayalite) at ambient conditions and transforms
254 directly into spinel (γ-Fe_2SiO_4, ahrensite) under high pressure at ambient temperature. Silicate spinels have
255 been known as an essentially metastable phase at ambient conditions.
256 There are several passes of spinel structure transformations. Some oxide spinels with transition elements have
257 their high-pressure polymorphs due to the transition without decomposition. A pseudo-rhombohedral phase
258 at pressures above 30 GPa and ambient temperature was reported on the basis of powder diffraction data and
259 Mössbauer data (Greenberg et al., 2011). However, structure parameters including atomic positional
260 parameters of the high-pressure phase are not reported in their paper and their Rietveld analysis at 48(2) GPa
261 did not consider the residual spinel phase in the refinement. Hence, several peaks are not clearly fitted.
262 Present paper shows a structural change in Fe_2SiO_4 spinel under high pressure up to 64 GPa. A new
263 high-pressure structure of *I*-Fe_2SiO_4 is determined by Rietveld profile fitting of synchrotron x-ray diffraction
264 data at ambient temperature. A transition from the cubic spinel structure to a body centered orthorhombic
265 phase (*I*-Fe_2SiO_4) with space group *Imma* and Z=4 was first observed at approximately 39 GPa. The
266 structure of *I*-Fe_2SiO_4 has two crystallographically distinct FeO_6 octahedral sites and Si atom changes its
267 configuration.
268 In addition to the new structure, we first found two different compression curves of the lattice parameter
269 in the spinel phase and the discontinuity at approximately 20 GPa. Fe-$K\beta$ x-ray emission measurements at
270 elevating pressure show that the transition from high-spin (HS) state to intermediate-spin (IS) state begins at
271 17 GPa in the spinel phase. The IS electronic state is gradually enhanced with pressure, which generates an
272 isostructural change in the lattice parameter at 20 GPa. The spin transition induces the compression of the
273 bond length, resulting in the structure transition at 39 GPa. The spin transition can be emphasized for
274 the trigger of the structure transition.
275

276 **Acknowledgments**

277 We express our great thanks to Prof. E. Ito of Okayama University, Japan for providing us Fe_2SiO_4 spinel
278 samples. This work was sponsored by the Carnegie/DOE Alliance Center (CDAC, DE-FC52-08NA28554).
279 Support from DOE-BES (DE-FG02-06ER46280) Energy Frontier Research Center funded by the U.S.
280 Department of Energy (DOE), Office of Science, The present investigation was also performed under the

281 auspices of KEK proposals No. 2004G229 for powder diffraction at BL-13A and BL-18C of the Photon
282 Factory, Tsukuba, Japan

283

284 **References**

285

286 Geophysical Research Letters, **38**, L08309,(1999) Magnetism in FeO at megabar pressures from x-Ray
287 emission spectroscopy. Physical Review Letters, **83**, 4101–4104.
288 Burnley, P.C., Green, H.W., and Prior, D. (1991) Faulting associated with the olivine to spinel transformation in
289 Mg_2GeO_4 and its implications for deep-focus earthquakes. Journal of Geophysical Research, **B96**, 425–443.
290 Derzsi, M. Piekarz, P., Tokár, K., Jochym, P.T., Łaewski, J., Sternik, M., and Parlinski, K. (2011) Comparative
291 *ab initio* study of lattice dynamics and thermodynamics of Fe_2SiO_4- and Mg_2SiO_4-spinels. Ding, Y., Haskel, D.,
292 Ovchinnikov, S.G., Tseng, Y.C., Orlov, Y.S., Lang, J.C., and Mao, H.K. (2008) Novel pressure-induced
293 magnetic transition in magnetite (Fe_3O_4)..
294 . Journal Geophysical Research, **B96**, 2157–2169.
295 Pressure-induced structural phase transition of the iron end-member of ringwoodite (γ-Fe_2SiO_4) investigated by
296 x-ray diffraction and Mössbauer spectroscopy.
297 Science, **279**, 1698–1700.
298
299
300 Katsura, T., and Ito, E. (1989) The system Mg_2SiO_4-Fe_2SiO_4 at high pressure and temperature: Precise
301 determination of stabilities of olivine, modified spinel and spinel.
302 Geophysical Research Letters, **24**, 2841–2844.
303
304 Leven, J.H., Jackson, I., and Ringwood, A.E. (1981) Upper mantle seismic anisotropy and lithospheric
305 decoupling.
306 Li, L., Cares, P., and Weidner, D.J. (2007) Effect of cation ordering and pressure on spinel elasticity by *ab*
307 *initio* simulation.
308
309 Lin, J.F., Struzhkin, V.V., Jacobsen, S.D., Hu, M.Y., Chow, P., Kung, J., Liu, H., Mao, H.K., and Hemley, R.J.
310 (2007) X-ray emission spectroscopy with a laser-heated diamond anvil cell: a new experimental probe of the
311 spin state of iron in the Earth's interior.

312 Lin, J.F., Struzhkin, V.V., Jacobsen, S.D., Shen, G., Spin transition of iron in magnesiowüstite in the Earth's
313 lower mantle.
314 Liu, Q., Liu, W., Whitaker, M.L., Wang, L., and Li, B. (2008) Compressional and shear wave velocities of
315 Fe_2SiO_4 spinel at high pressure and high temperature.
316 Mao, H.K., J., and Bell, P.M. (1986) Calibration of the ruby pressure gauge to 800-kbar under quasi-hydrostatic
317 conditions. Journal Geophysical Research, **B91**, 4673- 4676.
318
319 Mattila, A., Rueff, J.P., Badro, J., Vankó, G., Shukla, A., (2007) Metal-ligand interplay in strongly correlated
320 oxides: a parameterized phase diagram for pressure-induced spin transitions.
321 ., Barnett, J.D., and Forman, R.A. (1975) Calibration of the pressure dependence of the R1 ruby fluorescence
322 line to
323 A and de Groot, F.M.F. (2006) Probing the 3d spin momentum with x-ray emission spectroscopy: The case of
324 molecular-spin Transitions.
325

Table captions

Table 1.

Lattice parameters were determined by Rietveld profile fitting analysis. Spinel phase is found at pressures above the transition pressure of 38.8 GPa and coexists with the high-pressure phase of *I*-Fe_2SiO_4.

Table 2.

Table 3.

Reliability factors for the least-squares calculation are

$$wR_p = \left[\frac{\Sigma_i w_i |y_i - f_i(x)|}{\Sigma_i w_i y_i}\right]^{1/2} . \quad R_p = \left[\frac{\Sigma_i |y_i - f_i(x)|}{\Sigma_i y_i}\right]$$

$$R_F = \left[\frac{\Sigma_k |F_{k\,obs}| - |F_{k\,cal}|}{\Sigma_k F_{k\,obs}}\right] \qquad s = \left[\frac{\Sigma_i w_i |y_i - f_i(x)|}{N - P}\right]^{1/2}$$

Table 4.

Figure captions

Figure 1. Selected x-ray diffraction patterns of Fe_2SiO_4 taken with increasing pressure at ambient temperature.

The high-pressure phase was found above 39 .2 GPa and observed up to 56.6 GPa.

Figure 2.

There are two distinct compression regimes indicating the boundary at about 20 GPa. This behavior is a little higher pressure than the HS-to-IS transition of 17 GPa observed by XES. The data of Greenberg et al. (2011) are also presented. The dotted curve represents the lattice parameter of the residual spinel coexist with *I*-Fe_2SiO_4. The observed error is smaller than the data point.

Figure 3. Average bond length ratio of tetrahedral and octahedral sites of Fe_2SiO_4 spinel.

Bond lengths were obtained from the Rietveld profile fitting method. Error is smaller than the symbol mark. The Fe-O bond length in the octahedral site confirms the two different compression regimes at 20 GPa.

Figure 4. The decompression experiment confirms a reversible transition between cubic and orthorhombic phases. Subsequent laser heating at 1500 K and 31 GPa reveals decomposition from spinel to rhombohedral FeO and SiO_2 stishovite. Reflections with symbols of I and in the figure represent *I*-Fe_2SiO_4 and spinel phase, respectively.

Figure 5. Rietveld profile fitting of the initial structure model of rhombohedral Fe_2SiO_4 to the data obtained at 54.6 GPa. The rhombohedral structure model (space group $R\bar{3}m$) is simply derived from a distortion along the <111]> direction of the spinel structure. Peaks indicated by the arrows are not indexed.

Figure 6. Rietveld profile fitting of diffraction data obtained at 54.6 GPa, assuming a two-phase mixture of orthorhombic Fe_2SiO_4 and spinel. Upper and lower vertical bars indicate peak positions for orthorhombic Fe_2SiO_4 and spinel, respectively.

Figure 7. Rietveld profile fitting of diffraction data obtained at 64 GPa. Rietveld profile fitting was carried out in consideration of two-phase mixture of *I*-Fe_2SiO_4. . Vertical bars indicate peak positions of the *I*-Fe_2SiO_4.

Figure 8. There are two distinct octahedral Fe sites, Fe1 and Fe2. Si also is located at the site of octahedral coordination. Fe1 and Fe2 octahedra create layers parallel to (011) respectively. SiO_6 octahedra make an array in the direction of <100]>.

Figure 9.

Fe_2SiO_4 spinel (ringwoodite ahrensite) and high-pressure phase *I*-Fe_2SiO_4 are presented in the left and right figure, respectively. Arrow indicates a martensitic transformation with translation vector $<\vec{1/8}\ \vec{1/8}\ \vec{1/8}>$, which generates the *I*-Fe_2SiO_4 structure from the spinel. The shadowed circles in the left figure represent the atomic positions of *I*-Fe_2SiO_4.

Figure 10. Fe $K\beta$ x-ray emission spectra with increasing pressure up to 64.8 GPa. The upper left figure shows the expanded $K\beta'$ spectra, indicating an intermediate spin transition. The spin transition occurs at approximately 17 GPa.

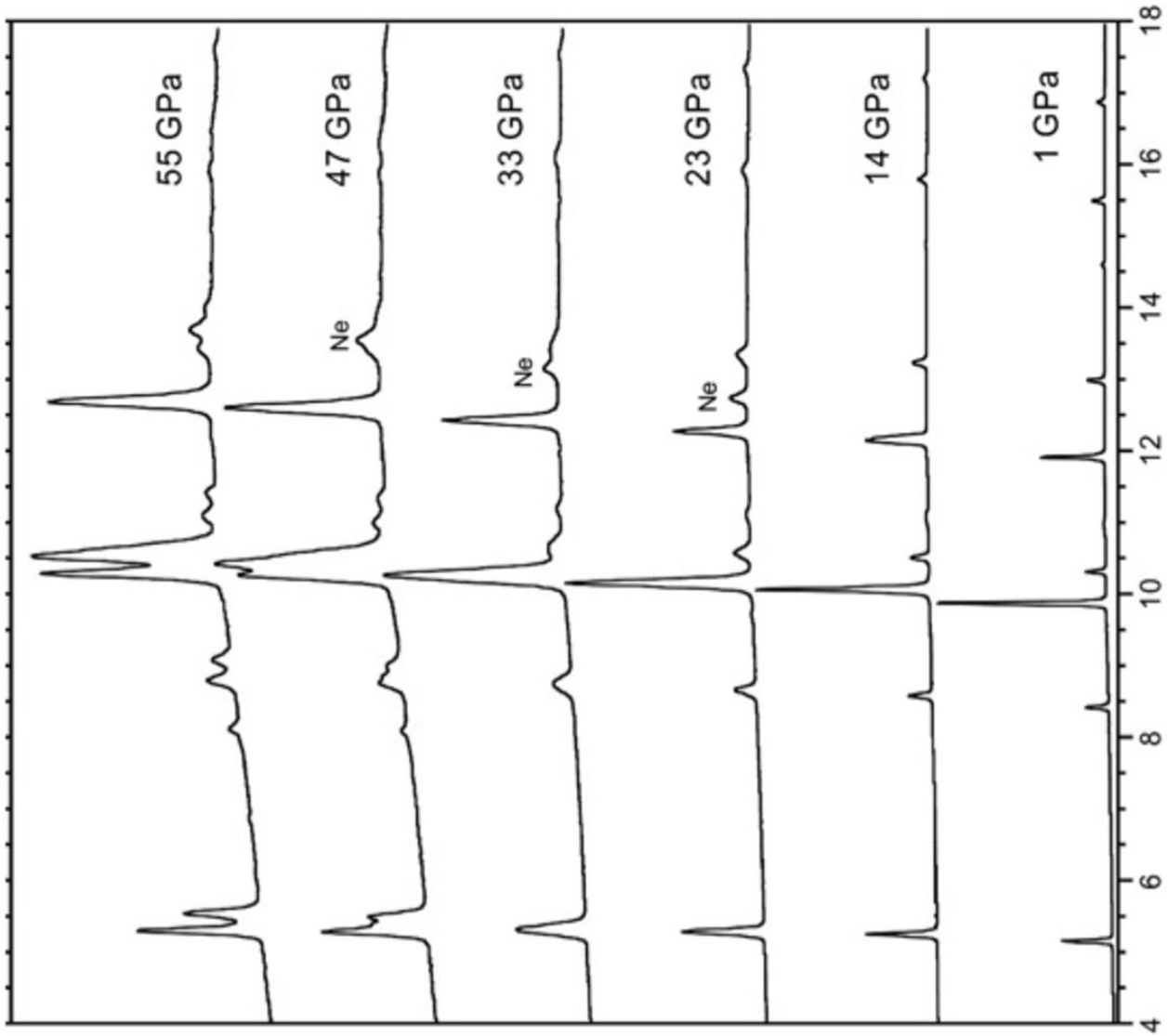
55 GPa
47 GPa
Ne
33 GPa
Ne
23 GPa
Ne
14 GPa
1 GPa
4
6
8
10
12
14
16
18
2θ (λ=0.4262 Å)

Fig. 1

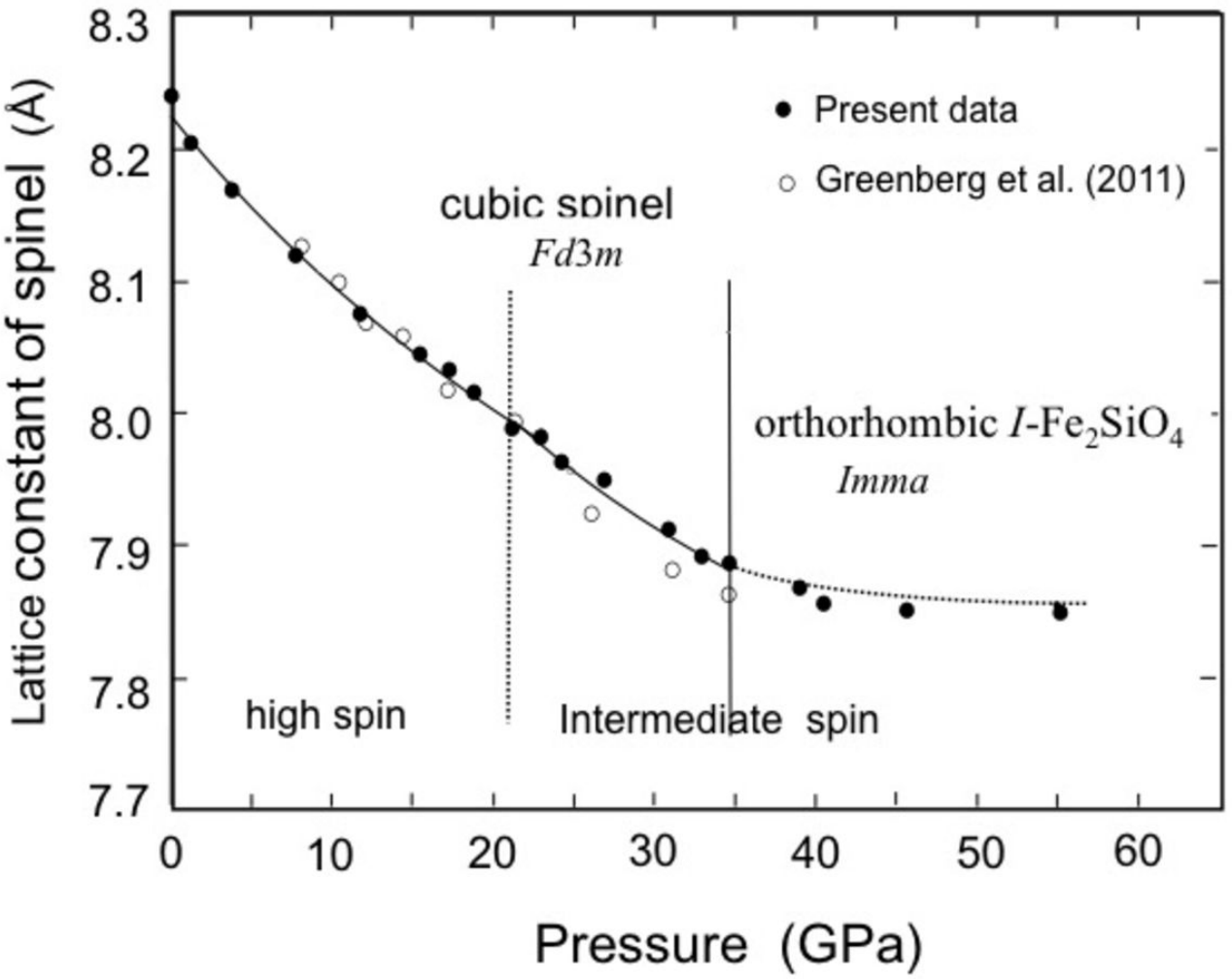
Lattice constant of spinel (Å)
8.3
8.2
8.1
8.0
7.9
7.8
7.7
0
10
20
30
40
50
60
Pressure (GPa)
Present data
Greenberg et al. (2011)
cubic spinel
Fd3m
orthorhombic I-Fe2SiO4
Imma
high spin
Intermediate spin

Fig. 2

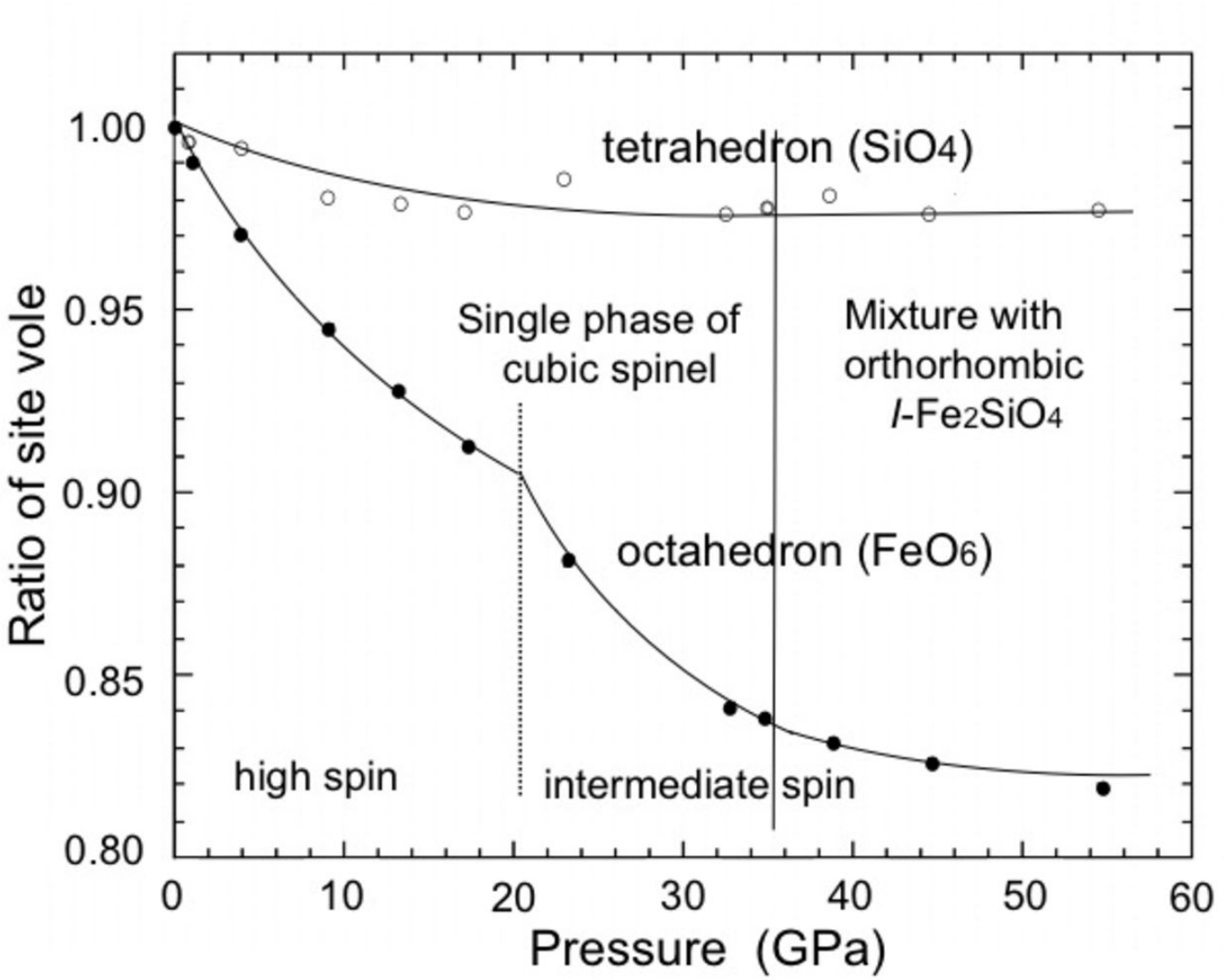
1.00
0.95
0.90
0.85
0.80
Ratio of site vole
0
10
20
30
40
50
60
Pressure (GPa)
tetrahedron (SiO4)
Single phase of
cubic spinel
Mixture with
orthorhombic
I-Fe2SiO4
octahedron (FeO6)
high spin
intermediate spin

Fig. 3

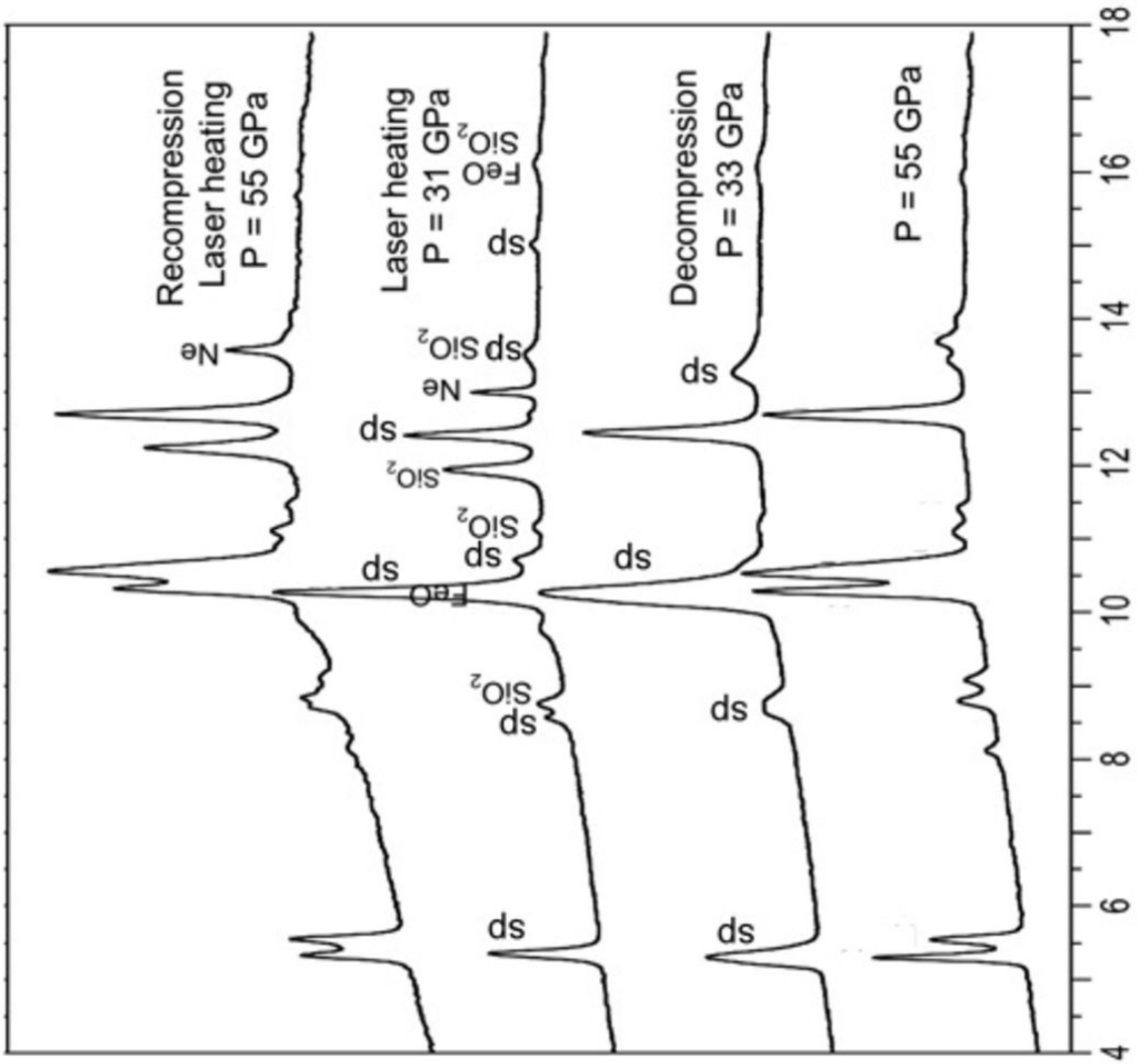
Recompression
Laser heating
P = 55 GPa
Laser heating
P = 31 GPa
Decompression
P = 33 GPa
P = 55 GPa
Ne
sp
ds
SiO2
FeO
TeO
2θ (λ=0.4262 Å)
4
6
8
10
12
14
16
18

Fig. 4

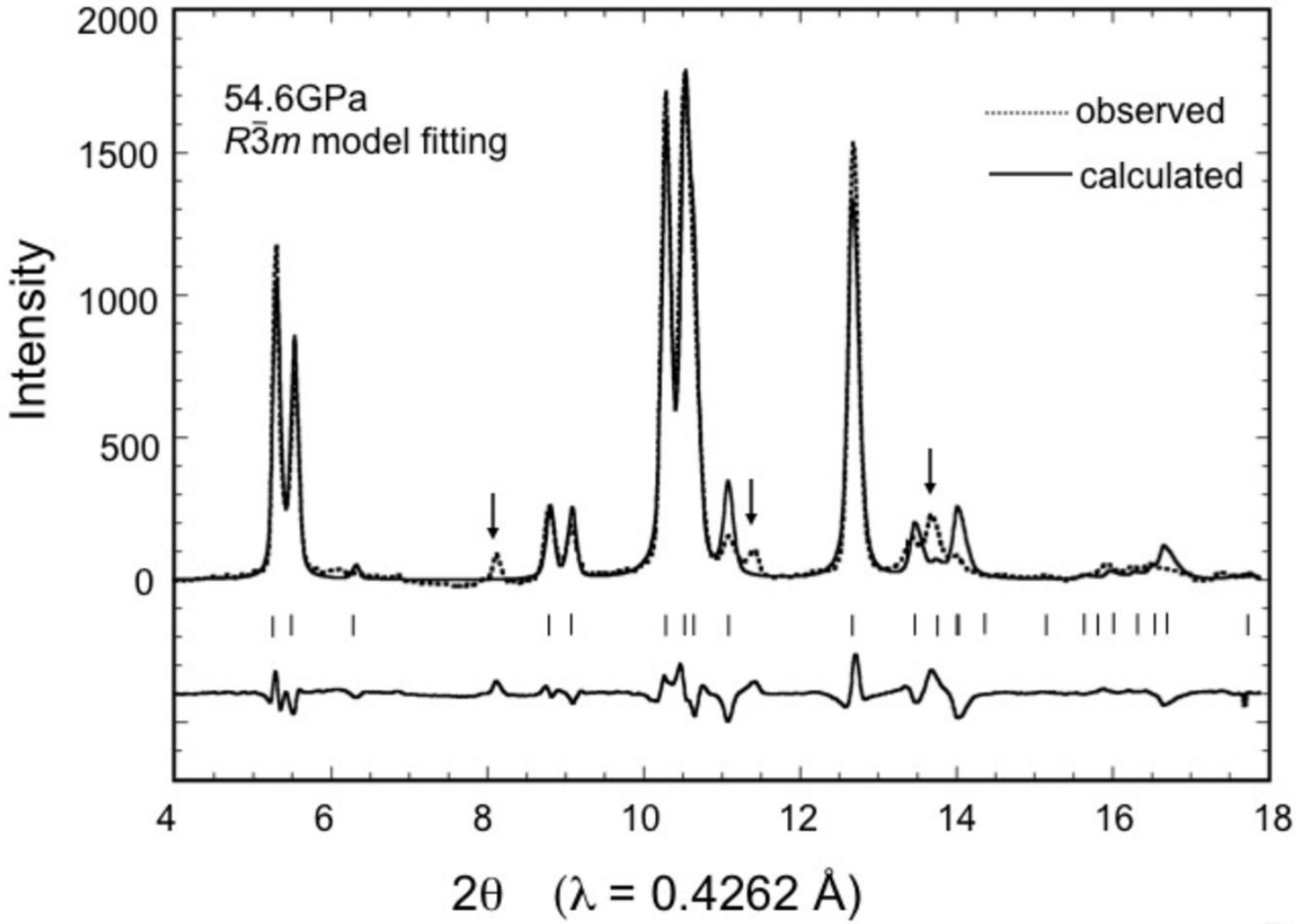
54.6GPa
$R\bar{3}m$ model fitting
observed
calculated
Intensity
2000
1500
1000
500
0
4
6
8
10
12
14
16
18
2θ (λ = 0.4262 Å)

Fig. 5

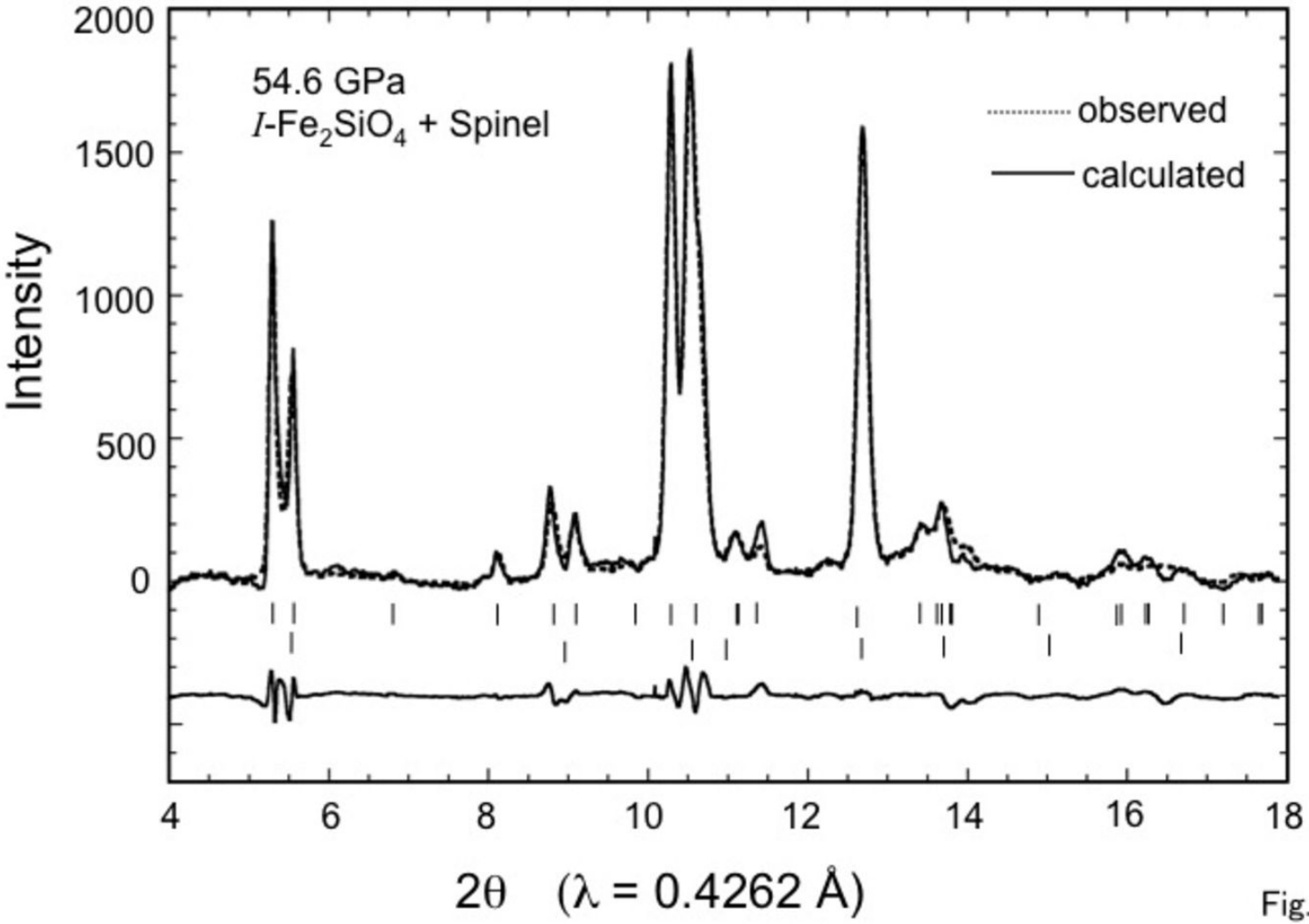
54.6 GPa
I-Fe2SiO4 + Spinel
observed
calculated
Intensity
2000
1500
1000
500
0
4
6
8
10
12
14
16
18
2θ (λ = 0.4262 Å)

Fig. 6

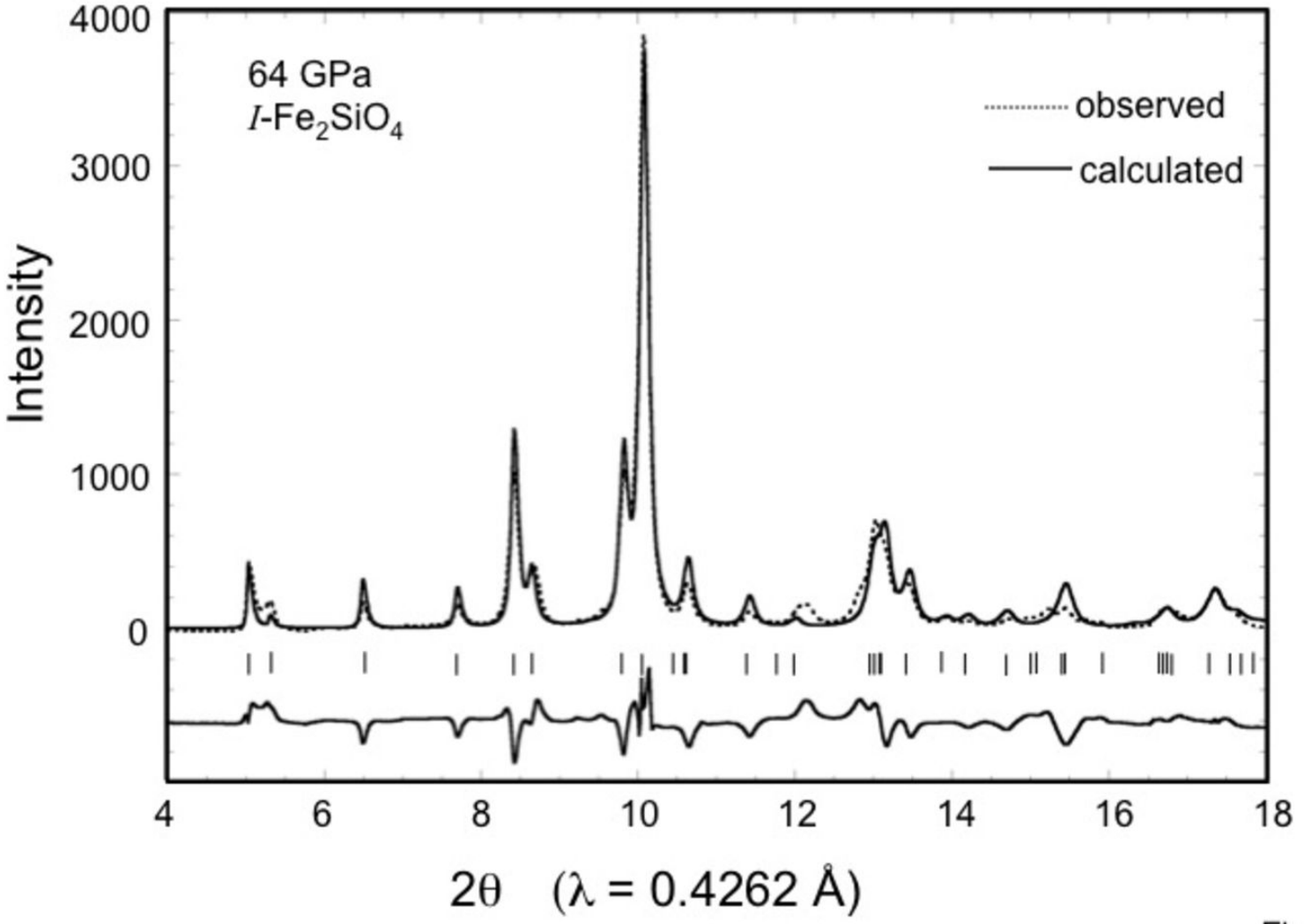
64 GPa
I-Fe2SiO4
observed
calculated
Intensity
4000
3000
2000
1000
0
4
6
8
10
12
14
16
18
2θ (λ = 0.4262 Å)

Fig. 7

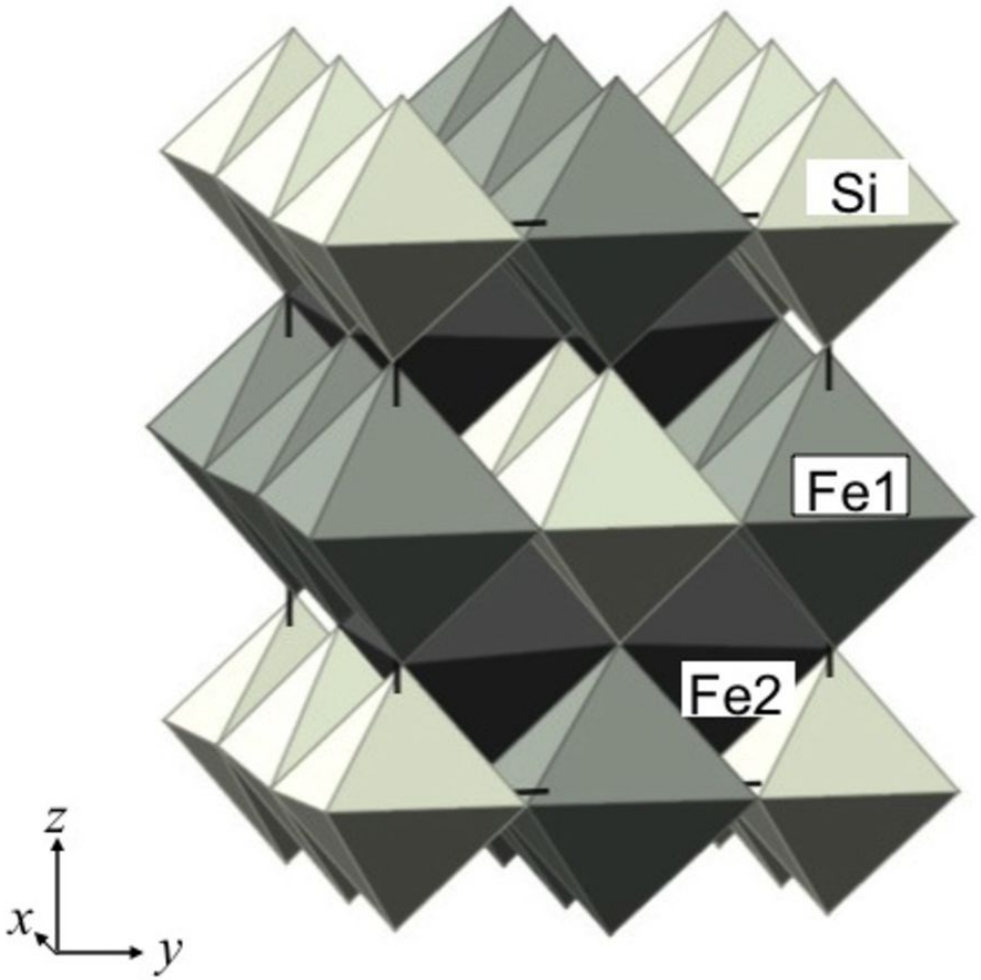

Fig. 8

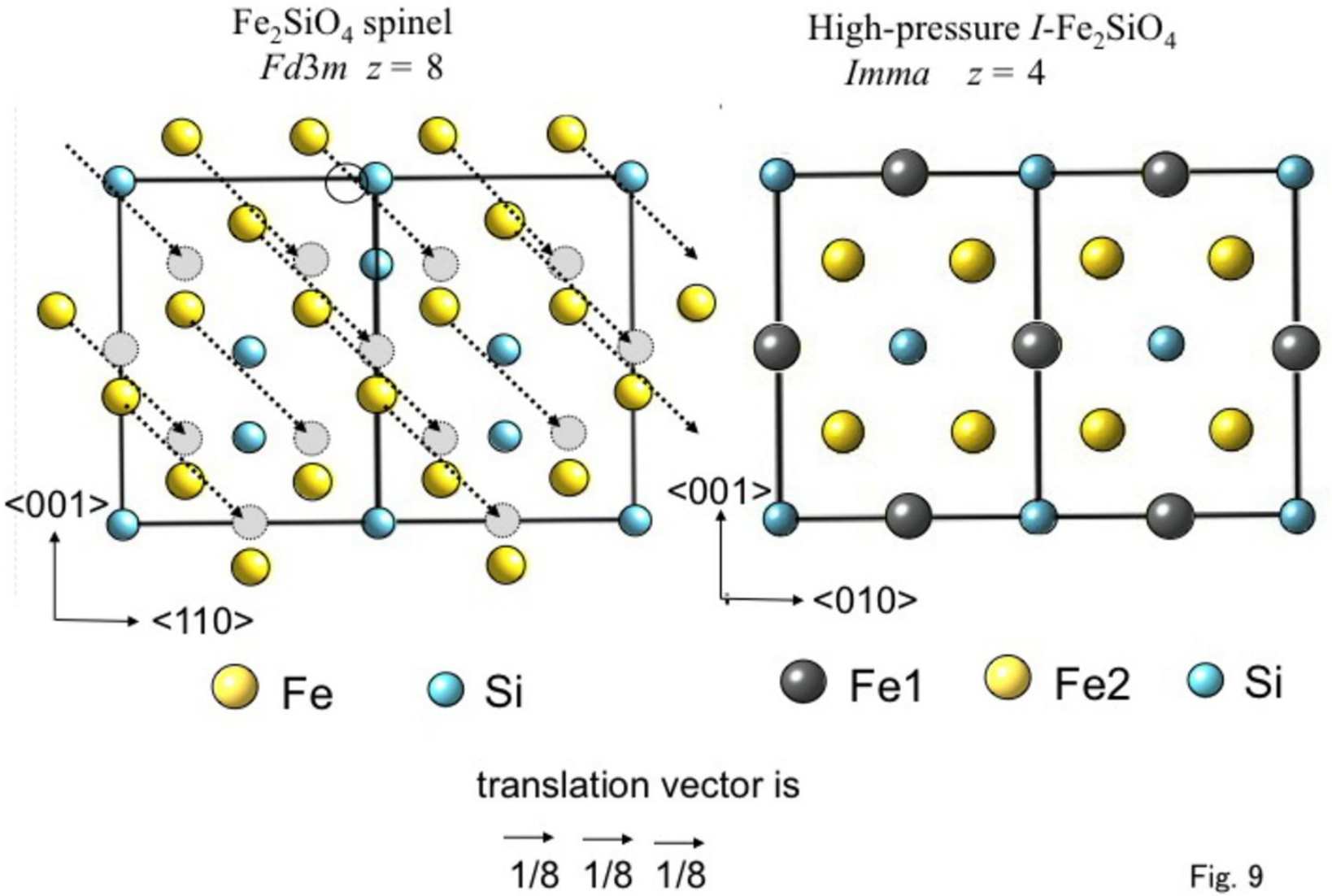
Fe_2SiO_4 spinel
$Fd3m$ $z = 8$
High-pressure I-Fe_2SiO_4
$Imma$ $z = 4$
<001>
<110>
<001>
<010>
Fe
Si
Fe1
Fe2
Si
translation vector is
1/8 1/8 1/8

Fig. 9

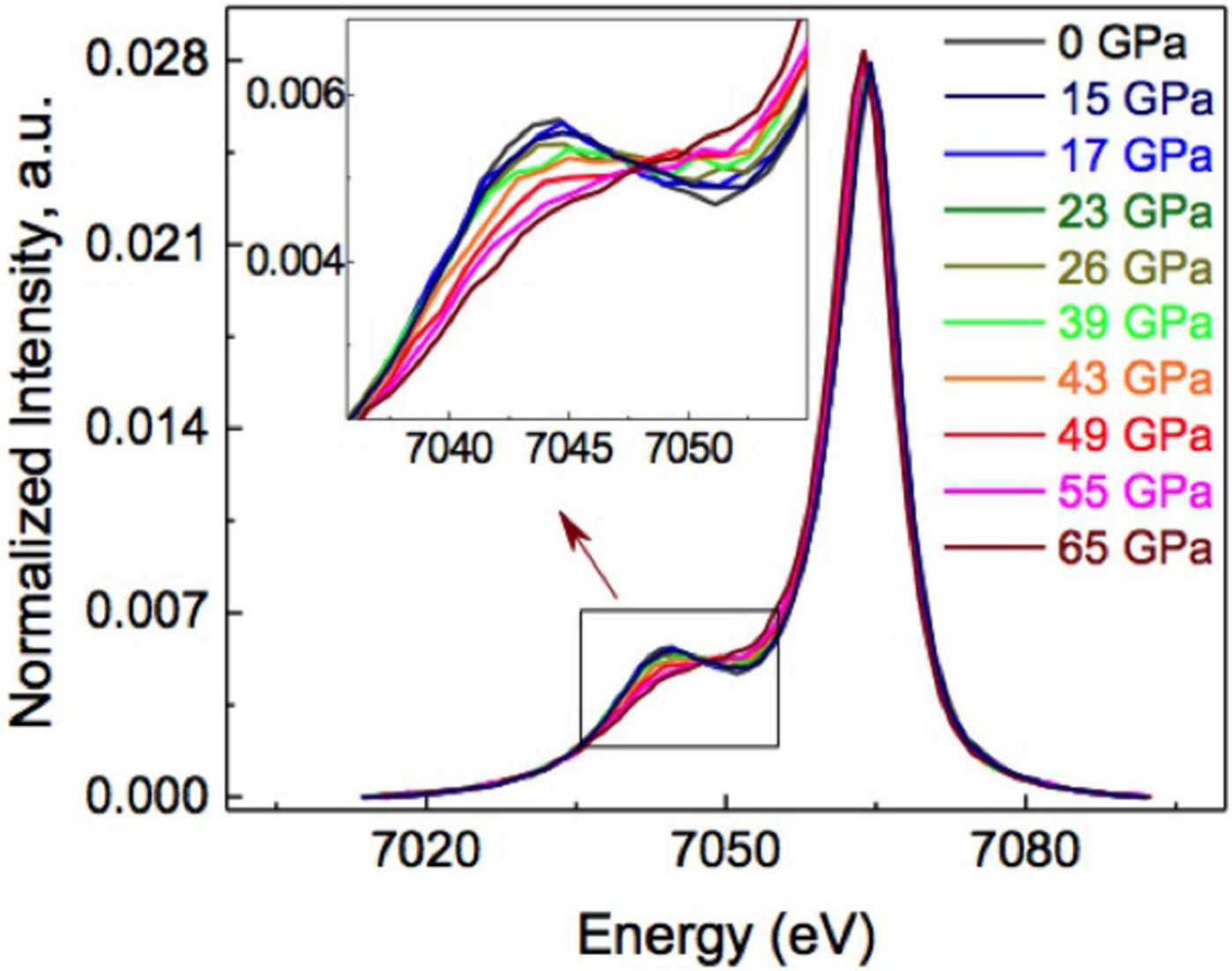
Normalized Intensity, a.u.
0.028
0.021
0.014
0.007
0.000
7020
7050
7080
Energy (eV)
0.006
0.004
7040
7045
7050
0 GPa
15 GPa
17 GPa
23 GPa
26 GPa
39 GPa
43 GPa
49 GPa
55 GPa
65 GPa

Fig. 10

Table 1 Lattice constant of Fe_2SiO_4 spinel

P (GPa)	LC (Å)	P (GPa)	LC (Å)
spinel stable region		two-phase mixuture	
		metasatble spinel	
0.0001	8.2374 (4)	38.8	7.859(4)
1.2	8.2156 (8)	39.2	7.855(4)
3.7	8.1783 (9)	44.6	7.756(2)
4.0	8.1759 (8)	54.6	7.730(2)
7.8	8.1325 (8)		
9.1	8.1140 (8)		
11.5	8.0905 (8)		
13.3	8.0759 (9)		
15.4	8.057 (1)		
17.3	8.044 (1)		
18.8	8.028 (1)		
20.3	8.013 (1)		
22.3	7.996 (1)		
23.1	7.990 (1)		
24.2	7.976 (2)		
27.2	7.951 (2)		
31.0	7.916 (2)		
32.9	7.895 (2)		
34.8	7.889 (3)		

Table 2 Bond distance and site volume of spinel phase under pressure

Press GPa	Cell const Å	Cell vol Å^3	u-parameter	d(Si-O) Å	d(Fe-O) Å	Vol(SiO4) Å^3	Vol(FeO6) Å^3
0.0001	8.2374(4)	558.95(6)	0.3659(2)	1.654(7)	2.137(7)	2.321(2)	12.914(2)
1.2	8.2156(8)	554.52(7)	0.3661(2)	1.652(6)	2.130(6)	2.314(4)	12.784(3)
4.0	8.1759(8)	546.46(8)	0.3666(2)	1.651(6)	2.115(6)	2.310(2)	12.530(2)
9.1	8.1142(8)	533.81(7)	0.3670(2)	1.644(7)	2.096(6)	2.282(3)	12.197(3)
13.3	8.0759(5)	526.71(5)	0.3673(8)	1.641(5)	2.083(5)	2.267(1)	11.986(1)
17.3	8.044(1)	520.5(2)	0.3678(9)	1.641(17)	2.071(17)	2.269(9)	11.779(9)
23.1	7.990(1)	510.0(2)	0.3692(11)	1.650(18)	2.045(18)	2.304(12)	11.368(13)
32.9	7.895(3)	492.1(1)	0.3700(11)	1.641(13)	2.014(13)	2.268(12)	10.868(13)
34.8	7.889(3)	490.9(1)	0.3702(13)	1.642(12)	2.011(12)	2.274(22)	10.818(23)
			metastable spinel above the transition pressure				
38.8	7.879(4)	489.1(1)	0.3705(25)	1.644(17)	2.006(17)	2.272(23)	10.74(23)
39.2	7.855(4)	484.7(1)	0.3711(22)	1.648(16)	1.995(16)	2.295(23)	10.57(23)
44.6	7.756(2)	466.6(3)	0.3707(15)	1.622(12)	1.973(12)	2.188(16)	10.22(16)
54.6	7.730(2)	461.9(2)	0.3708(11)	1.617(10)	1.966(10)	2.171(14)	10.11(14)

Table 3 Structure parameters of high-pressure phase of *I*-Fe_2SiO_4

Pressure			44.6GPa*	54.6GPa*	64.8GPa
Space group			*Imma*	*Imma*	*Imma*
Unit molecule			4	4	4
a	(Å)		5.551(3)	5.543(1)	5.522(3)
b	(Å)		6.030(4)	6.032(2)	6.025(4)
c	(Å)		7.241(5)	7,201(4)	7.185(5)
volume	($Å^3$)		242.4(4)	240.8(2)	239.0(2)
Rwp			2.996	2.531	2.369
R_B			1.993	1.354	7.573
R_F			0.985	1.042	4.088
s			0.4047	0.3436	1.8538
Si	4a	x	0.0	0.0	0.0
		y	0.0	0.0	0.0
		z	0.0	0.0	0.0
		Biso	4.83(2)	4.87(2)	2.05(2)
Fe1	4b	x	0.0	0.0	0.0
		y	0.0	0.0	0.0
		z	0.5	0.5	0.5
		Biso	6.74(1)	3.54(1)	2.90(1)
Fe2	4c	x	0.25	0.25	0.25
		y	0.25	0.25	0.25
		z	0.25	0.25	0.25
		Biso	4.92(1)	3.88(3)	2.92(5)
O1	8h	x	0.0	0.0	0.0
		y	0.5101(9)	0.5073(5)	0.5068(9)
		z	0.7652(9)	0.7608(8)	0.7610(8)
		Biso	3.6531)	4.00(1)	3.72(2)
O2	8i	x	0.2371(9)	0.2342(8)	0.2333(2)
		y	0.25	0.25	0.25
		z	0.0022(9)	0.0014(9)	0.0012(6)
		Biso	5.91(2)	6.24(5)	5.54(5)

Table 4 Deformation of Si, Fe1 and Fe2 octahedra of *I*-Fe_2SiO_4

Pressure			44.6GPa	54.6GPa	64.8GPa
Si	O1	x 2 (Å)	1.701(4)	1.723(4)	1.718(4)
	O2	x 4 (Å)	2.001(4)	1.990(4)	1.982(4)
	mean	(Å)	1.901(4)	1.901(4)	1.894(4)
	volume	($Å^3$)	8.99(6)	8.99(6)	8.89(4)
Fe1	O1	x2 (Å)	1.921(5)	1.879(3)	1.876(3)
	O2	x4 (Å)	2.098(5)	2.108(3)	2.107(3)
	mean	(Å)	2.039(5)	2.032(3)	2.030(3)
	volume	($Å^3$)	11.26(6)	11.13(5)	11.09(5)
Fe2	O1	x4 (Å)	2.008(6)	2.017(6)	2.015(4)
	O2	x2 (Å)	1.796(6)	1.792(6)	1.790(4)
	mean	(Å)	1.937(6)	1.942(8)	1.940(4)
	volume	($Å^3$)	9.58(4)	9.66(2)	9.61(2)